# Collective excitations and mode coupling in layered superconductors

H. A. Fertig and S. Das Sarma
*Center for Theoretical Physics and Center for Superconductivity Research, Department of Physics, University of Maryland, College Park, Maryland 20742*
(Received 7 March 1991)

We investigate the collective-mode spectrum for a layered superconductor structure. For wave vectors directed close to the superlattice axis, we find that the plasmon modes remain *below* the superconducting gap edge. This is in sharp contrast with the situation for isotropic superconductors in three dimensions, for which the Anderson-Higgs mechanism lifts all such modes out of the gap. We also find that, as a mode crosses the gap edge, either by increasing the wave vector or tilting its direction with respect to the superlattice axis, there is a unique mode-coupling effect between pair-breaking excitations and the collective mode. This manifests itself as a line splitting in the dielectric response, which may in principle be used to determine the gap of such a system. We also calculate the effect of interplane tunneling on the collective-mode spectrum. We find that, if the tunneling rate is large enough, the plasmon modes may all be lifted out of the gap. We show that estimates for the plasmon energy based on the effective-mass approximation can grossly *overestimate* its minimum value.

## I. INTRODUCTION

Since the discovery of high-$T_c$ superconductors, intense investigations have focused on how the layered structure of these materials determines and affects their properties.[1] The anisotropy introduced by this structure can be extremely pronounced: the effective-mass ratio $m_z/m$, where $m$ is the mass for motion within a plane and $m_z$ is for motion between planes, has been reported as high as $3\times10^3$ in bismuth-based compounds,[2] and more recently as at least $10^5$ in thallium-based compounds.[3] Furthermore, one can, in principle, make the mass anisotropy as large as one wants in artificially grown superconducting superlattices, where the distances between superconducting layers may be chosen by the sample grower.[4]

A natural question to ask about such systems is what is the collective mode spectrum, given that the system is layered and exhibits superconductivity? After all, for semiconductor superlattices, it is well known that the layered structure completely changes the plasmon dispersion from its isotropic counterpart.[5,6] In what follows, we will investigate, in detail, the collective-mode spectrum for the superconducting superlattice system, working in the BCS approximation with $s$-wave pairing. This work follows up an earlier short publication by the present authors,[7] providing some details of that work as well as some additional results.

One of the most interesting results of this investigation is that, if the tunneling between planes is small enough, it necessarily follows that there are plasmon modes whose energy is less than the gap, $2\Delta$. This is a unique result because it is generally believed that there are no electronic excitations below the gap in a clean, isotropic ($s$-wave) BCS superconductor.[8,9] The behavior of the latter type of system directly follows from the Anderson-Higgs mechanism,[8] which is essentially a screening effect, and hence is dependent upon the detailed form of the three-dimensional Fourier transform of the Coulomb potential, $4\pi e^2/\kappa q^2$, where $q$ is the wave vector and $\kappa$ the appropriate dielectric constant. By contrast, the appropriate Coulomb interaction for a layered system is softer[5] at small $q$, so that the Anderson-Higgs mechanism is not completely effective in these systems. It is thus clear that the absence of modes in the gap for isotropic superconductors is a question of detail, rather than physical necessity.[10,11]

A typical example of our calculated plasmon dispersion $\omega(\mathbf{k})$ is shown in Fig. 1. Here we have chosen sys-

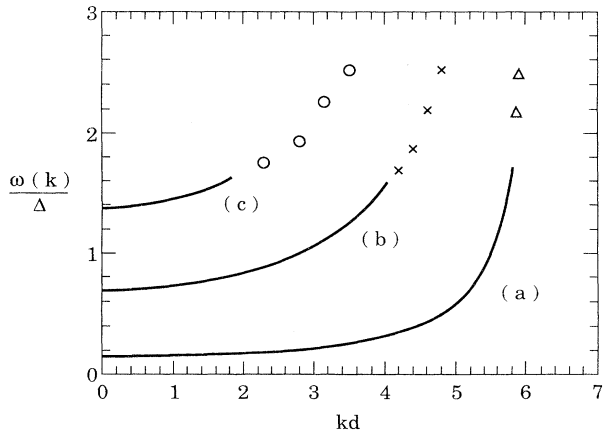


FIG. 1. Plasmon dispersion $\omega(\mathbf{k})/\Delta$. Solid lines are obtained using expansions in $v_F k_\parallel/\Delta$ for (a) $\theta=0.01$, (b) $\theta=0.05$, and (c) $\theta=0.1$ rad. All other points are obtained by numerical integration of Eqs. (12). Triangles correspond to $\theta=0.01$, crosses to $\theta=0.05$, and open circles to $\theta=0.1$. Material parameters chosen are $n_s=1.0\times10^{14}$ cm$^{-2}$, $m^*=5m_0$, $\kappa=4$, $d=10$ Å, and $T_c=125$ K.

 

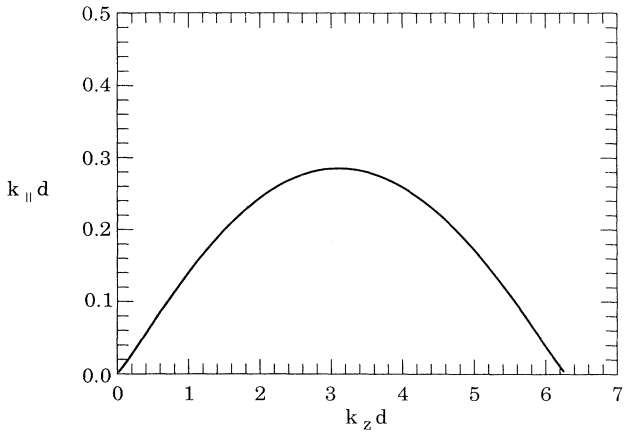


FIG. 2. Wave vectors for which the plasmon mode lies in the gap; the region below the curve indicates where the modes are present. The diagram is periodic in $k_z d$ with period $2\pi$. Only data for $0 \leq k_z d \leq 2\pi$ are shown. Material parameters are the same as in Fig. 1.

tem parameters appropriate to model a hypothetical high-$T_c$ superconductor: sheet density $n_s = 10^{14}$ cm$^{-2}$, interplane distance $d = 10$ Å, in-plane effective mass $m^* = 5m_0$, where $m_0$ is the bare electron mass, $\kappa = 4$, and $T_c = 125$ K. The unit of energy here is half the gap $\Delta$ which, in the BCS approximation, is given by $\Delta = 1.76 k_B T_c$. In this example, tunneling between planes is ignored. The dispersion is quite sensitive to the propagation angle $\theta$, defined as the angle between the $k$ vector and the superlattice axis. For small $\theta$, we see that $\omega(k) < 2\Delta$ in the long-wavelength limit. For these parameters, we find that $\omega(k) < 2\Delta$ at small $k$ for $\theta < \theta_c$, where $\theta_c \simeq 8°$. This behavior can be summarized by a "phase diagram" such as that shown in Fig. 2, which shows the wave vectors for which these modes are below the gap edge at $2\Delta$.

We have also calculated the density response function $\chi(\mathbf{k},\omega)$, which is essentially the dielectric response of this system to electromagnetic radiation. We find a very unusual phenomenon when the plasmon mode crosses $2\Delta$. This behavior is illustrated in Fig. 3, where we plot the absorptive part of the dielectric response, Im$\chi$, as a function of $\omega$ for fixed $\mathbf{k}$.

For $\omega(k) < 2\Delta$, we see a sharp $\delta$-function peak in Im$\chi$, representing the plasmon mode, and a small broader peak above $2\Delta$, arising from pair-breaking excitations. As $k$ is increased such that $\omega(k)$ crosses $2\Delta$, we obtain a line splitting in Im$\chi$, arising from mode coupling between the collective mode and pair-breaking modes.[7,12] As $k$ is further increased, a large plasmonlike peak moves out to large energies, while a smaller peak remains at $2\Delta$. We note that, although this behavior is illustrated here for fixed $\theta$ and increasing $k$, the same phenomenon will arise if one fixes $k$ and increases $\theta$ until the plasmon energy $\omega(\mathbf{k})$ crosses $2\Delta$. Thus, this line splitting should occur in the long-wavelength limit ($kd \ll 1$), and would be observed if one can detect the plasmon mode at a given $\mathbf{k}$, and then tilt the sample with respect to $\mathbf{k}/k$ until $\omega(\mathbf{k})$ exits the gap. One important byproduct of an observation of this phenomenon would be a unique and direct identification of the energy gap, since the leading edge of one of the two peaks always remains at $2\Delta$.

Finally, we have examined in detail the effect of interplane tunneling on the dispersion relations for these modes. We find that modes with $\mathbf{k}$ directed close to the superlattice axis are very sensitive to the presence of such tunneling in the long-wavelength limit. In particular, we find that if one plots $\omega(\mathbf{k})$ for fixed $k_z$ as a function of $k_\parallel$, a gap opens up at $k_\parallel = 0$ of order $W$, where $W$ is the interplane tunneling matrix element. By contrast, $\omega(\mathbf{k})$ vanishes at $k_\parallel = 0$ when $W = 0$. An example of this behavior is illustrated in Fig. 4. This means that the introduction of enough interplane tunneling will push the plasmon mode out of the gap. Such behavior is not surprising, since as one increases $W$, the system becomes more three dimensional, in which case we expect the Anderson-Higgs mechanism to become effective in producing a gap or a mass in the plasmon spectrum. For the parameters of Figs. 1–4, we expect that collective modes will still be present in the gap if $W < 0.23\Delta$ for a clean, layered system at $T = 0$. An estimate for the Y-Ba-Cu-O materials based on a measured mass anisotropy of $m_z/m_\parallel = 100$ gives $W \simeq 0.0075\Delta$, well within the range for which such modes should remain in the gap. For the cases of Bi-based[2,13] and Tl-based[3] materials, the mass anisotropies have been measured to be 1 and 3 orders of magnitude larger than this, making the prospects for subgap modes in these materials extremely good. However, we note that direct measurements of $W$ in these materials are not readily available, so that one should not take our estimate for $W$ too literally. With this caveat in mind, it is important to notice that estimates of the plasma frequency for $\theta = 0$, $k \to 0$ computed directly from the effective-mass approximation[14] [i.e., $\omega_p^2 = 4\pi e^2 \rho / m_z$] can grossly *overestimate* the minimum value of $\omega(\mathbf{k})$.

It is natural to ask whether such modes are readily observable in electromagnetic absorption experiments such as infrared absorption[15] and Raman scattering.[6] To date, we are not aware of any experiments clearly showing the results discussed in this work. This is not surprising, however, because nearly all absorption experiments on single-crystal samples of high-$T_c$ materials have worked with $\mathbf{E}$, the electric field of the light, in the $a$-$b$ plane. In this situation, the $\mathbf{k}$ vector is strictly along the $c$ axis, and the oscillator strength of our predicted plasmon mode turns out to vanish (for $W = 0$) in this limit. In general, the oscillator strength for the subgap plasmon modes scales as $(k_\parallel d)^2$, where $d$ is the interlayer spacing, so that one needs to look at modes propagating at an angle with respect to the $c$ axis. Our belief is that the best system to look for these modes is in artificially layered superconductors,[4] where $d$ may be made as large as one likes, both increasing the oscillator strength (for a fixed $k$) and decreasing the value of $W$.

This article is organized as follows. In Sec. II we will review the Nambu formalism and its application to layered systems. In Sec. III, we develop expansions for the dielectric response valid in the long-wavelength limit, and show how one may determine the subgap plasmon disper-

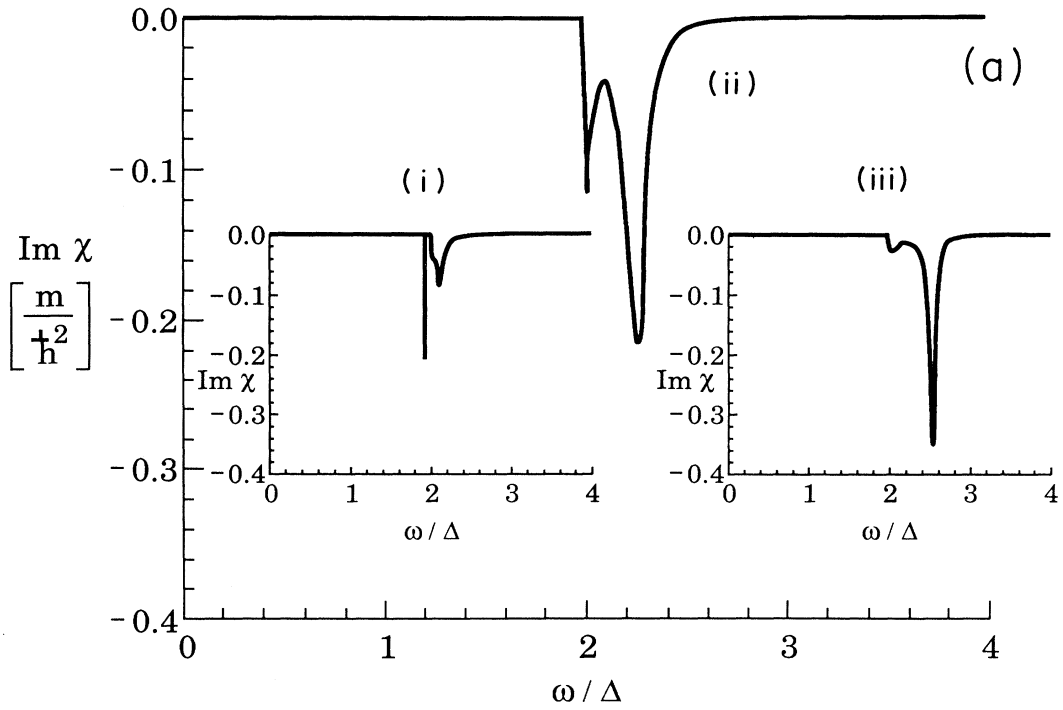


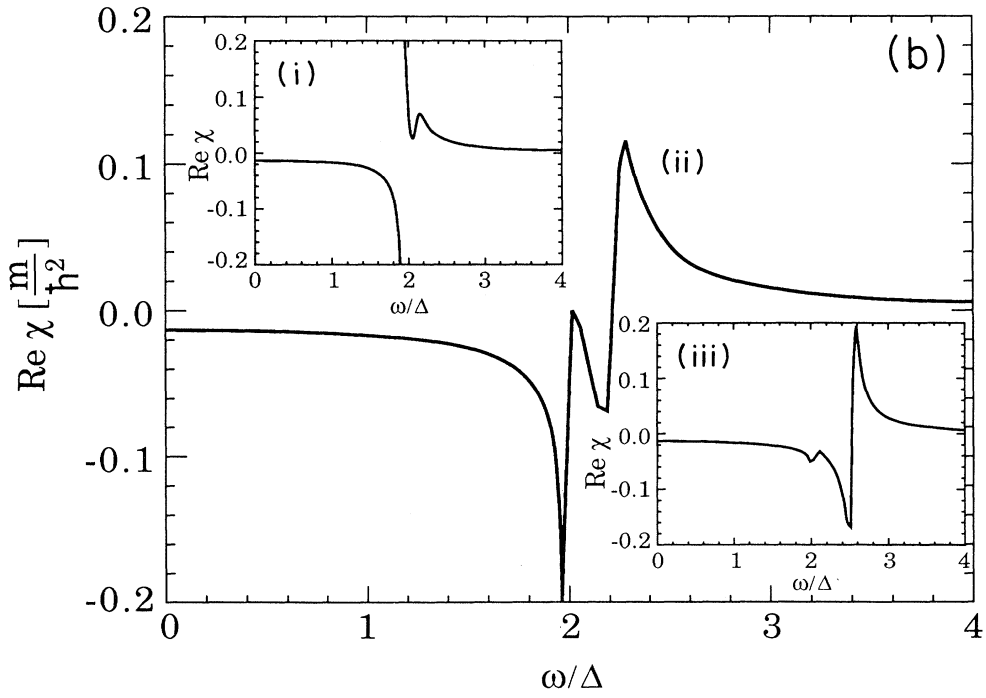


FIG. 3. (a) Absorptive part of dielectric response as a function of unitless frequency, $\omega/\Delta$, in units of $m/\hbar^2$. Material parameters as in Fig. 1, $\theta=0.1$, and (i) $kd=2.8$ (sharp line represents a $\delta$ function at the position of the plasmon pole), (ii) $kd=3.15$, and (iii) $kd=3.5$. (b) Reactive part of the dielectric response.

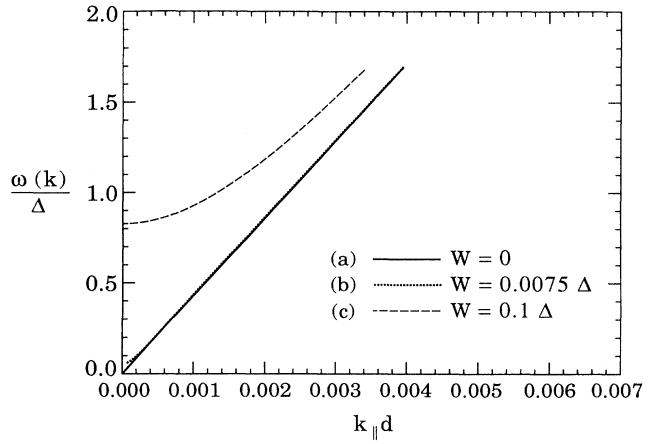


FIG. 4. Plasmon dispersion $\omega(\mathbf{k})$ for fixed $k_z$ as a function of $k_\parallel d$ for different values of the tunneling rate $W$. Material parameters as in Fig. 1, (a) $W=0$, (b) $W=0.0075\Delta$, and (c) $W=0.1\Delta$.

sions from those. In Sec. IV we present numerical results for the dielectric function, valid at larger values of $k$, and discuss, in detail, the mode-coupling effect. Section V discusses the effect of interlayer tunneling on the plasmon dispersions. We conclude in Sec. VI with a summary.

## II. FORMALISM

In this section, we briefly review the Nambu formalism[16,17] and its application to layered superconductors with no interplane tunneling, and show how it is used to derive the density response of the system. Our starting Hamiltonian may be written in the form $H \equiv H_0 - \mu N + H_{\rm int}$, with

$$H_0 - \mu N = \sum_i \sum_{\mathbf{k}} \bar{\varepsilon}_k \Psi_{\mathbf{k},i}^\dagger \tau_3 \Psi_{\mathbf{k},i} ,$$

$$H_{\rm int} = \tfrac{1}{2} \sum_{i,j} \sum_{\substack{\mathbf{p}_1,\mathbf{p}_2 \\ \mathbf{q}\neq 0}} (\Psi_{\mathbf{p}_1+\mathbf{q},i}^\dagger \tau_3 \psi_{\mathbf{p}_1,i}) v_{ij}(q) (\Psi_{\mathbf{p}_2-\mathbf{q},j}^\dagger \tau_3 \psi_{\mathbf{p}_2,i}) .$$

Here, $\Psi_{\mathbf{k},i}^\dagger \equiv (c_{\mathbf{k},i\uparrow}^\dagger, c_{-\mathbf{k},i\downarrow})$, $c_{\mathbf{k},i\sigma}^\dagger$ creates an electron in the $i$th layer with spin $\sigma$ in the state $\mathbf{k}$th momentum state ($\mathbf{k}$ here is a two-dimensional vector in the $x$-$y$ plane; the superlattice axis is taken to lie along the $\hat{\mathbf{z}}$ direction). The quantity $\bar{\varepsilon}_k \equiv k^2/2m - \mu$, and $\tau_3$ is the usual Pauli spin matrix. The interparticle potential is taken for simplicity to be

$$\tilde{v}_{ij}(\mathbf{q}) = \frac{2\pi e^2}{\kappa q} e^{-q|i-j|d} - V_0 \delta_{ij} , \tag{1}$$

where $d$ is the interplane spacing, $\kappa$ the dielectric constant, the first term is just the two-dimensional Fourier transform of the Coulomb interaction for electrons confined to planes a distance $|i-j|d$ apart, and the last term represents a weak, short-ranged attractive potential.[17] This form is essentially the usual weak-coupling BCS approximation as applied to a layered structure. The quantity of interest here is the density response function, whose poles give the collective mode energies. It is defined as

$$\chi(k_\parallel, k_z, \omega) = -i \int_0^\infty dt\, e^{i\omega t} \langle [\rho(\mathbf{k},t), \rho(-\mathbf{k},0)] \rangle ,$$

where $\rho(\mathbf{k},t)$ is the three-dimensional Fourier transform of the density operator in the Heisenberg representation. In the Nambu formalism, this is written as

$$\chi(k_\parallel, k_z, \omega) = -i \int_{-\infty}^{\infty} dt\, e^{i\omega t} \frac{1}{dL^2} \sum_{\substack{p_1,p_2, \\ q}} \sum_j \langle T \Psi_{\mathbf{p}_1,j}^\dagger(t) \tau_3 \Psi_{\mathbf{p}_1-\mathbf{k}_\parallel j}(t) \Psi_{\mathbf{p}_2,0}^\dagger \tau_3 \Psi_{\mathbf{q}_2,0} \rangle ,$$

where $L^2$ is the surface area of a plane. We next perform a diagrammatic expansion of $\chi$ in terms of the interaction $H_{\rm int}$. The density response may be written in terms of an irreducible polarizability as shown in Fig. 5. A key observation here is that, because of the absence of interplane tunneling, the interaction [Eq. (1)] cannot scatter electrons into different planes. This means the solution to the equation shown in Fig. 5 is

$$\chi(k_\parallel, k_z, \omega) = \frac{\Pi(k_\parallel, \omega)}{1 - \tilde{v}(k_\parallel, k_z)\Pi(k_\parallel, \omega)} , \tag{2}$$

where $\Pi(k_\parallel, \omega)$ is the irreducible polarizability for a single, isolated sheet, and

$$\tilde{v}(k_\parallel, k_z) \equiv \sum_j \frac{2\pi e^2}{\kappa k_\parallel} e^{-k_\parallel dj + i k_z dj} - V_0 \equiv \frac{2\pi e^2}{\kappa k_\parallel} \frac{\sinh(k_\parallel d)}{\cosh(k_\parallel d) - \cos(k_z d)} - V_0 . \tag{3}$$

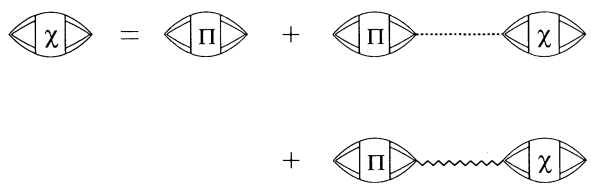


FIG. 5. Diagrammatic representation of the dielectric response in terms of the irreducible polarizability Π. Dotted line represents contact interaction, the way line represents the Coulomb interaction, the double lines are Green's functions with self-energy corrections, which are matrices in the Nambu formalism. Each Green's function carries a layer index; since the interactions do not scatter electrons into different planes, each nonvanishing diagram must have the same layer index in all three Green's functions.

The fact that $\Pi$ is manifestly diagonal in the layer index is a great simplification because it allows us to write the density response of the superlattice system in terms of the polarizability of an isotropic, two-dimensional system via Eq. (2). The superlattice structure here enters only through the form of $\tilde{v}(k_\parallel,k_z)$ shown in Eq. (3).

To evaluate $\Pi$, it is necessary to construct a gauge-invariant, number-conserving approximation in order to get the collective-mode spectrum. This is accomplished by choosing diagrams that are consistent with the form of the self-energy correction[9,10,11,17] to the Green's functions (which in the Nambu formalism is a matrix). Figure 6(a) shows the diagrams we include in the self-energy matrix.[16,17] The last contribution, which is an exchange self-energy, must be kept in order to include the superconducting instability. The second diagram, which is the direct Hartree term, vanishes in the presence of a uniform neutralizing background charge. We note that this form for the self-energy amounts to a self-consistent Hartree approximation in the Coulomb interaction, and a self-consistent Hartree-Fock approximation in the contact interaction.[18] Because an exchange term has to be kept in the self-energy, one must include, consistent with the Ward identity, ladder diagrams in the polarizability in order to get a gauge-invariant result. Our approximation for the polarizability is shown in Fig. 6(b). It may be written in the form

$$\Pi(k,\omega)=-i\,\mathrm{Tr}\int\frac{d\omega_1 d^2p_1}{(2\pi)^3}\tau_3\underline{G}(p_1,\omega_1)\Gamma(p_1,k,\omega)\times\underline{G}(\mathbf{p}_1-\mathbf{k},\omega_1-\omega)\,, \tag{4}$$

where the Green's functions $\underline{G}$ are $2\times2$ matrices, and $\Gamma$ is a vertex matrix. Because of the simple form we have chosen for the attractive part of the potential, the vertex part (which in our approximation is the sum of ladder diagrams) satisfies the equation

$$\Gamma(p_1,k,\omega)=\tau_3+iV_0\tau_3\int\frac{d^2q\,d\omega_1}{(2\pi)^3}\underline{G}(q,\omega_1)\Gamma(q,k,\omega)\times\underline{G}(\mathbf{q}-\mathbf{k},\omega_1-\omega)\tau_3\,. \tag{5}$$

One can easily see from Eq. (5) that $\Gamma(p_1,k,\omega)$ has no $p_1$ dependence. Writing

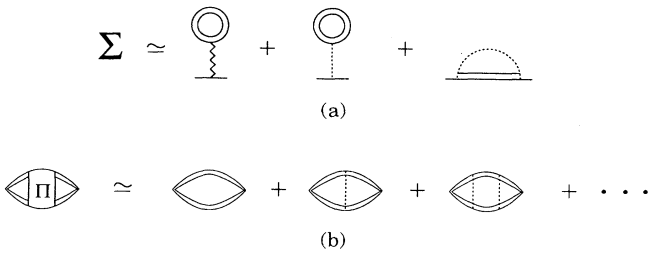


FIG. 6. (a) Self-consistent equation for self-energy correction. (b) approximation used for polarizability, which generates a gauge-invariant result of the dielectric response.

$$\Gamma(k,\omega)\equiv\tau_3+iV_0\underline{M}(k,\omega) \tag{6}$$

defines a matrix $M$, which satisfies

$$\underline{M}(\mathbf{k},\omega)=\int\frac{d^2q\,d\omega_1}{(2\pi)^3}\tau_3\underline{G}(q,\omega_1)[\tau_3+i\underline{M}(k,\omega)]\times\underline{G}(\mathbf{q}-\mathbf{k},w_1-\omega)\tau_3\,. \tag{7}$$

Equations (6) and (7) show that the vertex part can be found by solving a linear matrix equation rather than an integral equation, as at first seems the case in Eq. (5). The solution to Eq. (7) is found by expanding $\underline{M}$ in the Pauli spin matrices: $\underline{M}=\sum_{i=0}^{3}M_i\tau_i$, and then equating the coefficients of the $\tau_i$'s on both sides of the equation. We drop terms of $O(\Delta/E_F)$, where $\Delta$ is the order parameter, satisfying the BCS equation

$$\Delta=V_0\int\frac{d^2q}{(2\pi)^2}\frac{\Delta}{2Eq}\,, \tag{8}$$

where $E_q^2\equiv\bar{\varepsilon}_q^2+\Delta^2$. [This equation is derived in the Nambu formalism by solving the self-consistent equations for the self-energy in Fig. 6(a). The integral in Eq. (8) is formally divergent; this will be discussed below.] After much algebra, one finds that $M_0\simeq M_1\simeq0$, and

$$\begin{aligned}M_2&=-i\omega G-iV_0F_-M_2+\omega V_0GM_3\,,\\ M_3&=F_++\omega V_0GM_2+iV_0F_+M_3\,,\end{aligned} \tag{9}$$

where

$$\begin{aligned}G(\mathbf{k},\omega)&=\Delta\int\frac{d\omega_1d^2q}{(2\pi)^3}\frac{1}{(\omega_1+\frac{1}{2}\omega)^2-E^2_{\mathbf{q}+1/2\mathbf{k}}}\frac{1}{(\omega_1-\frac{1}{2}\omega)^2-E^2_{\mathbf{q}-1/2\mathbf{k}}}\,,\\ F_\pm(\mathbf{k},\omega)&=\int\frac{d\omega_1d^2q}{(2\pi)^3}\frac{\omega_1^2-\frac{1}{4}\omega^2-\Delta^2\pm\bar{\varepsilon}_{\mathbf{q}+1/2\mathbf{k}}\bar{\varepsilon}_{\mathbf{q}-1/2\mathbf{k}}}{[(\omega_1+\frac{1}{2}\omega)^2-E^2_{\mathbf{q}+1/2\mathbf{k}}][(\omega_1-\frac{1}{2}\omega)^2-E^2_{\mathbf{q}-1/2\mathbf{k}}]}\,.\end{aligned} \tag{10}$$

Combining Eqs. (4), (6), and (9), one finally arrives at the result

$$\Pi(k,\omega)=\frac{2C(k,\omega)}{1-V_0C(k,\omega)}\,, \tag{11a}$$

where

$$C(k,\omega)=-iF_+(k,\omega)+\frac{V_0\omega^2G^2(k,\omega)}{1-iV_0F_-(k,\omega)}\,. \tag{11b}$$

Equations (10) and (11) are essentially the two-dimensional version of Prange's result,[10,11] and they share many of the properties of their three-dimensional counterparts. The frequency integrals in Eq. (10) may be handled analytically, leading to the forms

$$G(\mathbf{k},\omega)=-i\int\frac{d^2q}{(2\pi)^2}\frac{\Delta}{4E_{q+}E_{q-}}\times\left[\frac{1}{\omega-E_{q+}-E_{q-}+i\delta}-\frac{1}{\omega+E_{q+}+E_{q-}-i\delta}\right],$$
$$F_{\pm}(\mathbf{k},\omega)=-i\int\frac{d^2q}{(2\pi)^2}\frac{-E_{q+}E_{q-}-\Delta^2\pm\bar{\varepsilon}_{q+}\bar{\varepsilon}_{q-}}{4E_{q+}E_{q-}}\times\left[\frac{1}{\omega-E_{q+}-E_{q-}+i\delta}-\frac{1}{\omega+E_{q+}+E_{q-}-i\delta}\right], \tag{12}$$

where $\mathbf{q}_{\pm}\equiv\mathbf{q}\pm\frac{1}{2}\mathbf{k}$. The remaining task of our calculations, and the part in which the bulk of our work lies, is in finding various ways to evaluate Eq. (12). Before describing these, there is one important technical detail that must be clarified. One may notice that, in the limit $\omega,k\to 0$,

$$F_-(0,0)=-i\int\frac{d^2q}{(2\pi)^2}\frac{1}{2E_q}\ , \tag{13}$$

which, as it stands, is logarithmically divergent. The reason this divergence occurs is because we have chosen a point-contact potential for the attractive interaction, which has important contributions out to $q\to\infty$. Any real potential, however, will have some nonvanishing range, and in the original BCS approach this was modeled by integrating only over wave vectors $q$ such that $|\bar{\varepsilon}_q|\le\omega_D$, where $\omega_D$ is the Debye frequency. Such a cutoff should, in principle, be present in our integrals; however, taking the cutoff to infinity in Eqs. (12) introduces errors of $O(\Delta/\omega_D)$, which we will take to be small, with the sole exception being the case of $F_-$. We need not, however, introduce an explicit cutoff for this case.[11] Comparing Eq. (13) with Eq. (8) makes it clear that we may identify $F_-(0,0)=-i/V_0$. Thus, we can add $-i/V_0$ to and subtract the integral in Eq. (13) from our expression for $F_-(k,\omega)$. The resulting expression is perfectly finite when $\omega_D\to\infty$, so that taking this limit once again only introduces errors of $O(\Delta/\omega_D)$.

With this correction for $F_-$, we may now embark on our task of evaluating Eq. (12). We essentially have two approaches. The first involves expanding $G$ and $F_{\pm}$ for small values of $k$, which will prove useful for evaluating the plasmon dispersions inside the gap. These expansions, however, turn out to be invalid at frequencies greater than $2\Delta-v_Fk_{\parallel}/2$, where $v_F$ is the Fermi velocity. For larger wave vectors, it is necessary to evaluate Eqs. (12) directly. We will see that it is possible to express Re$G$ and Re$F_{\pm}$ in terms of elliptic integrals; the imaginary parts may be found then by a Kramers-Kronig transform. This latter technique turns out to be useful in illustrating the mode-coupling effect when the plasmon mode crosses the gap. In Sec. III below, we discuss the results from the long-wavelength expansion; in Sec. IV, we show the results of the Kramers-Kronig transform.

## III. SMALL-$k$ EXPANSIONS

Before discussing the full expansions of Eqs. (12), it is helpful to investigate the form of $\Pi$ and $\chi$ when both $\omega,k_{\parallel}^2/2m\ll 2\Delta$. In this case, we find

$$G\simeq\frac{im}{4\pi\Delta}\left[1-\frac{\omega^2}{6\Delta^2}-\frac{(v_Fk_{\parallel})^2}{12\Delta^2}\right],$$
$$F_{\pm}\simeq-\frac{im}{2\pi}\left[1+\frac{\omega^2}{4\Delta^2}\right],$$

and

$$F_-\simeq-\frac{i}{V_0}+\frac{im}{8\pi\Delta^2}[\tfrac{1}{2}(v_Fk_{\parallel})^2-\omega^2],$$

where $V_F$ is the Fermi velocity. Combining these forms with Eq. (11) yields

$$\Pi\cong\frac{(m/\pi)(v_0k_{\parallel})^2}{\omega^2-(1+mV_0/2\pi)(v_0k_{\parallel})^2}\ , \tag{14}$$

where $v_0\equiv v_F/\sqrt{2}$. The divergence in $\Pi$ at $\omega\approx v_0k_{\parallel}$ is the sound mode one expects in a neutral Fermi gas with weak attractive interactions. It is essentially the Goldstone mode associated with the broken gauge symmetry of the superconducting ground state. Substitution of Eq. (14) into Eq. (2) yields

$$\chi(k_{\parallel},k_z,\omega)=\frac{(m/\pi)(v_0k_{\parallel})^2}{\omega^2-[1+mV_0/2\pi+(m/\pi)\bar{v}(k_{\parallel},k_z)](v_0k_{\parallel})^2}+\mathcal{O}(k_{\parallel}^4,\omega^2k_{\parallel}^2,\omega^4)\ . \tag{15}$$

We thus find the plasmon poles in the limit $k_{\parallel}d\to 0$ at

$$\omega(k_{\parallel},k_z)\simeq\left[\frac{2me^2d}{k}\frac{1}{1-\cos k_zd}\right]^{1/2}v_0k_{\parallel}\ ,$$

for fixed $k_zd$. It follows that, for $k_{\parallel}\ll k_z$, one may always find a plasmon mode at arbitrarily small energy, in particular, with energy $\omega(k_{\parallel},k_z)<2\Delta$. We see then that our form for the polarizability, Eq. (14), forces upon us the presence of modes in the gap. It is worthwhile remarking that this form is actually quite general: the zero in the denominator appears because one has broken

gauge symmetry, and the fact that $\Pi(k_\parallel \to 0, \omega=0) \simeq k_\parallel^2$ is necessary to satisfy number conservation.[11] This means that the presence of modes in the gap is really quite general for the layered superconductor: it is independent of the pairing mechanism, and even of the appropriateness of the BCS approach. The only important assumption is that one may ignore tunneling between the planes. We will return to this point in Sec. V. Finally, we note that the factor $(v_0 k_\parallel)^2$ in the numerator of Eq. (15) implies that the oscillator strength for the plasmon mode actually vanishes as the **k** vector is directed closer and closer to the superlattice axis. This means that, although the lowest-energy modes are found in this situation, one needs to consider modes at higher $k$ or directed at an angle in order to maximize the coupling of the mode with an experimental probe.

We next expand Eqs. (12) for $k_\parallel^2/2m \ll 2\Delta$, with no assumption of small $\omega$. The resulting expansions are well behaved for $\omega < 2\Delta - v_F k_\parallel/2$. For values of $\omega$ approaching $2\Delta$, these expressions become divergent, indicating that $F_\pm$ and $G$ are not analytic in $k_\parallel^2$ when $\omega = 2\Delta$. The precise expressions are presented in Appendix A. With these expressions, one may find the poles of the density response function by finding the zeros of the denominator in Eq. (2). Figure 1 illustrates typical results for the plasmon dispersion $\omega(\mathbf{k})$, where here $\mathbf{k}=(\mathbf{k}_\parallel, k_z)$ for a fixed angle $\theta = \arctan k_z/k_\parallel$ as a function of the total wave-vector magnitude $k=(k_z^2+k_\parallel^2)^{1/2}$. In this example, we have used a hypothetical high-$T_c$ structure, roughly modeling Y-Ba-Cu-O, with sheet density $n_s = 10^{14}$ cm$^{-2}$, $d = 10$ Å, effective in-plane mass $m^* = 5m_0$, dielectric constant $\kappa = 4$, and $T_c = 125$ K. The gap $2\Delta$ is found via the usual BCS formula, $2\Delta = 3.52 k_B T_c$. To summarize the wave vectors for which there are plasmon modes in the gap, we would like to know the values of **k** such that $\omega(\mathbf{k}) = 2\Delta$. Unfortunately, this cannot be accomplished directly, because the expansions break down at this frequency. However, we find that, if one plots $\omega(\mathbf{k})$ versus $k_\parallel$ for fixed $k_z$, the result is extremely linear (see $W=0$ case of Fig. 4). This means it is a simple task to extrapolate the dispersion $\omega(\mathbf{k})$ for fixed $k_z$ to $\omega(\mathbf{k}) = 2\Delta$, thus giving us a value of $(k_\parallel, k_z)$ for which the plasmon mode crosses the gap. We note that direct numerical integration of $F_\pm$ and $G$ give values of **k** at which $\omega = 2\Delta$ in very good agreement with this extrapolation technique. The results of this calculation are presented in Fig. 2, where **k** values below the curve denote wave vectors for which $\omega(\mathbf{k}) < 2\Delta$, and points above satisfy $\omega(\mathbf{k}) > 2\Delta$. The curve is plotted for $0 \le k_z d \le 2\pi$; however, because $k_z d$ only enters $\bar{v}(k_\parallel, k_z)$ through $\cos(k_z d)$, it is clear that the phase diagram is actually periodic in $k_z d$. Because of this periodicity, a plasmon mode may actually leave and enter the gap several times as a function of $k$ for small angles $\theta$, as illustrated in Fig. 7. However, the angles necessary to achieve this situation are quite small, and are probably not physically relevant in most situations. Finally, we note that when tunneling is introduced ($W \neq 0$), the periodicity of the phase diagram is lost, and all modes in the gap with $k_z d > 2\pi$ may vanish even for relatively small values of $W$.

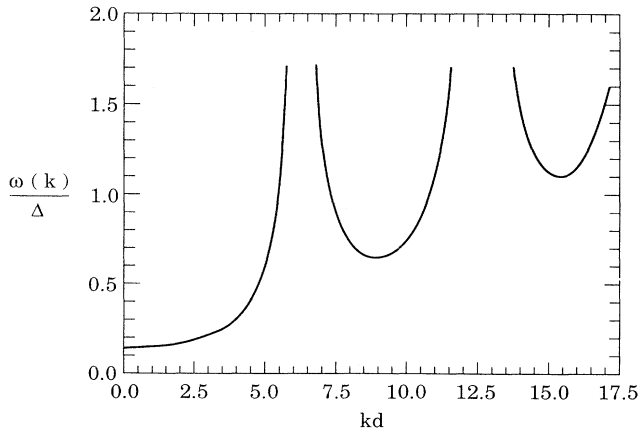


FIG. 7. Plasmon dispersion for $\theta = 0.01$, material parameters as in Fig. 1. For very small angles $\theta$, the plasmon mode may enter and exit the gap several times.

## IV. NUMERICAL RESULTS AND THE MODE-COUPLING EFFECT

For values of $\omega > 2\Delta - v_F k_\parallel/2$, the expansion method for evaluating $F_\pm$ and $G$ breaks down, and one needs to evaluate these functions exactly. The real parts of Eqs. (12) may be written in terms of elliptic integrals, for which excellent numerical packages already exist to evaluate them. One should note that $\mathrm{Re}G$, $\mathrm{Re}F_\pm = 0$ for $\omega < 2\Delta$; this is a direct statement of the existence of an energy gap for pair-breaking excitations. In Appendix B, we represent $\mathrm{Re}G$ and $\mathrm{Re}F_\pm$ in their elliptic integral representation. With Eqs. (B2)–(B4), it is possible to generate the imaginary parts $F_\pm$ via Kramers-Kronig transforms, such as

$$\mathrm{Im}X(k_\parallel,\omega) = \frac{-2}{\pi} \mathrm{P} \int_0^\infty \frac{\omega' \,\mathrm{Re}X(k_\parallel,\omega')}{\omega'^2 - \omega^2} d\omega' , \qquad (16)$$

where $X$ may be $G$ or $F_+$, and P here denotes a principle value integral. For the case of $F_-$, we need to treat the formally divergent part of the integral carefully. The proper expression in this case is

$$\mathrm{Im}F_-(k_\parallel,\omega) = -\frac{1}{V_0} - \frac{2}{\pi} \mathrm{P} \int_0^\infty d\omega' \left[ \frac{\omega' \,\mathrm{Re}F_-(k_\parallel,\omega)}{\omega'^2 - \omega^2} - \frac{\mathrm{Re}F_-(0,\omega')}{\omega'} \right] . \qquad (17)$$

The principal value integrals can be performed in the usual way, subtracting from the numerators of the form $\omega' \,\mathrm{Re}X(k_\parallel,\omega')$ their values at $\omega' = \omega$ to remove the singularity, and performing the integration of the subtracted term analytically. Some care must be taken, however, at the jump discontinuities in $\mathrm{Re}F_\pm$ and $\mathrm{Re}G$; direct integration over these introduces large errors in the numerical integration. One can overcome this by adding simple

functions to Re$F_{\pm}$ and Re$G$, such that the integral performed numerically has a continuous integrand, and then performing the principle value integral for the added functions analytically.[19]

Once the integrations have been performed, one can simply substitute the forms for $F_{\pm}$ and $G$ into Eqs. (11) to generate $\Pi$, and then use this form for $\Pi$ in Eq. (2) to generate the density response function.[20] We illustrate some typical results for the same material parameters as Fig. 1 in Fig. 8. Here we present $\chi$ as a function of $\omega$ for fixed $\mathbf{k}$; we take, for concreteness, $\theta=\arctan k_z/k_{\parallel}=0.05$ rad. For $kd=2.0$, one has a pole near $\omega=0.8\Delta$ in Re$\chi$; this translates into a $\delta$-function singularity at this frequency in Im$\chi$ which represents a plasma mode in the gap. For this wave vector, the plasmon contains nearly all the oscillator strength for absorption. There is also a peak in Im$\chi$ at $2\Delta$; this represents absorption via pair-breaking excitations, but by noting the scale at Im$\chi$ one can see that there is, in fact, very little oscillator strength in these excitations. For $kd=5.5$, one can see that the plasmon mode has moved out to $\omega\simeq 4.8\Delta$, and having exited the gap now has a finite width, corresponding to a finite lifetime for these collective excitations. There is some very small structure at $\omega=2\Delta$; this once again represents absorption by pair-breaking excitations with very low oscillator strength. We note that this behavior— dominance of the oscillator strength by the collective mode—is typical of dielectric functions at long wavelengths. This at first may seem surprising, since we are looking at $kd>1.0$; however, the relevant wavelength for such considerations is $k_{\parallel}d\equiv kd\sin\theta$, which for a small angle such as $\theta=0.05$ easily satisfys $k_{\parallel}d\ll 1$.

The behavior illustrated in Fig. 8 indicates that the plasmon mode shows little dependence on whether it lies either above or below the gap. One has a finite lifetime in the former case, leading to a broadened peak; however, the peak is actually quite sharp, and experimentally it might be difficult to distinguish the two cases. This might lead one to conclude that if the collective mode is observed and followed either as $kd$ is increased or $\theta$ is increased, then one might not know when and whether the mode has exited the gap. In fact, this is far from the case. In Fig. 3, we plot Im$\chi$ for values of $kd$ such that the collective mode just barely crosses the gap edge at $2\Delta$. One can see that strong mixing occurs between the collective mode and the pair-breaking excitations. This effect leads to the unusual line splitting visible in Fig. 3. Two important comments are in order here: first, the mixing of the pair-breaking and collective modes allows the former to play an important role in the dielectric absorption of the system; this is a unique situation, because we saw in Fig. 8 for $k_{\parallel}d\ll 1$, these excitations have a negligible oscillator strength. Second, the mode-coupling phenomenon seen here is unique to layered superconductors: one does not have it in normal layered systems, where pair-breaking excitations do not exist (i.e., there is no gap), and isostropic superconductors do not behave this way because the Anderson-Higgs mechanism pushes the collective mode far above the gap edge at $2\Delta$. As discussed in the Introduction, an observation of this phenomenon would allow a unique way to experimentally determine the gap of a system such as this, because one of the two peaks in the line-split dielectric response always remains at $2\Delta$.

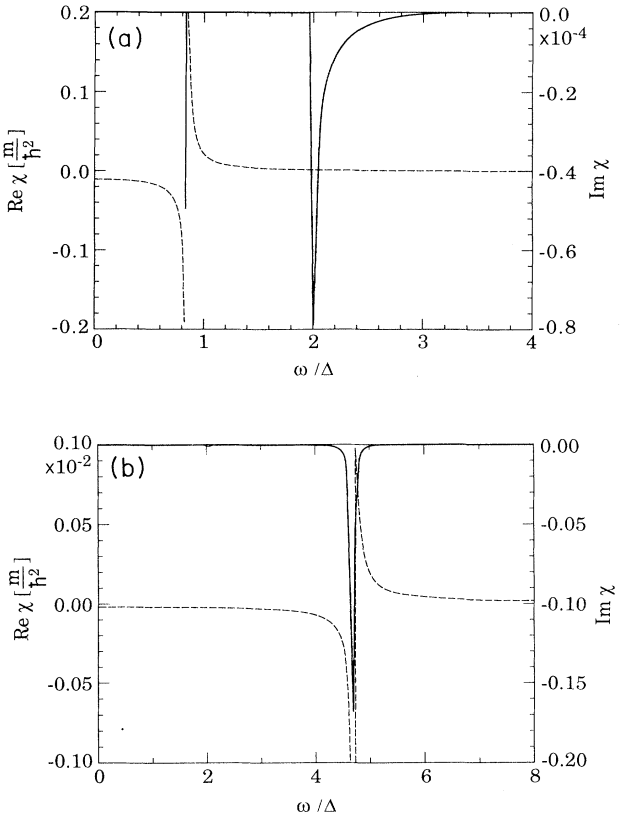


FIG. 8. (a) Dielectric response for $\theta=0.05$, $kd=2$, material parameters as in Fig. 1. Solid line is Im$\chi$, dashed line is Re$\chi$. (b) Dielectric response for $\theta=0.05$, $kd=5.5$.

To understand the mode-coupling phenomenon in more detail, it is helpful to examine the behavior of $\Pi(k_{\parallel},\omega)$ near $\omega=2\Delta$. The quantity $\Pi$ is actually qualitatively the same as the function $C(k_{\parallel},\omega)$ [cf. Eqs. (11)], and it is the latter quantity we will examine, because its value is independent of our choice of $V_0$. In Fig. 9, we illustrate Re$C$ for $k_{\parallel}d=0.315$, and material parameters as in Fig. 1. $C$ has a pole near $\omega=0$, which is the sound mode discussed in Sec. III associated with a neutral superconductor. On a scale that is reasonable for illustrating this pole, Re$C$ appears structureless near $\omega=2\Delta$; however, if we blow up this region, one actually finds two cusps in Re$C_1$: a downward cusp, located right at $\omega=2\Delta$, and an upward cusp at $\omega=(4\Delta^2+v_F^2k_{\parallel}^2)^{1/2}$. These cusps are associated with the pair-breaking excitations, and we will discuss their precise origin in a moment. That this structure occurs on such a fine scale here is not surprising, because we are in a regime (small $k_{\parallel}$) where the oscillator strength of the collective mode overwhelms that of the pair-breaking excitations. We note that similar structure was noted by Prange[9] for the three-dimensional isotropic superconductor.

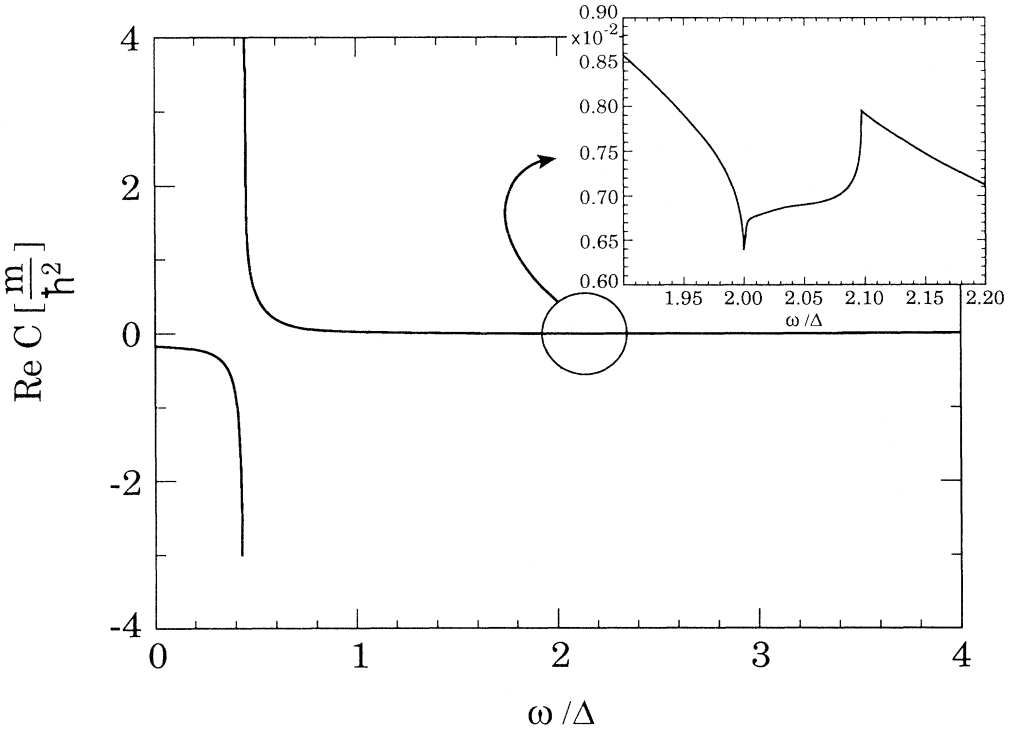


FIG. 9. Behavior of Re$C$ [cf., Eq. (11a)] for material parameters as in Fig. 1, with $\theta=0.1$, $kd=3.15$. On a coarse scale, Re$C$ appears smooth, but a blowup of the region near $\omega=2\Delta$ reveals two Van Hove singularities.

The structure near $\omega=2\Delta$ in $C$ translates into a very similar structure in $\Pi$, also existing only on a very fine scale. However, when we form $\chi$, the full dielectric response function, we get a huge amplification of this structure *if* the plasmon mode $\omega(\mathbf{k})$ is close to $2\Delta$. This is easily seen in Eq. (2): the plasmon mode frequency is given by a vanishing of the denominator on the right-hand side of this equation; since $\chi \propto \Pi$, the small denominator for $\omega \sim 2\Delta$ means that structure on a small scale in $\Pi$ is blown up to a much larger scale in $\chi$. There is no similar phenomenon in isotropic superconductors; in those materials, the plasmon mode is pushed up too far to ever allow this amplification phenomenon. Thus, we see that the suppression of the Anderson-Higgs mechanism by the layering effect allows one to actually probe structures in the dynamical response that would otherwise be difficult to see. Finally, we note that the fact that one of the two peaks present in Im$\chi$ is always centered at $2\Delta$ occurs because the downward cusp in Re$C$ is located precisely at $\omega=2\Delta$.

The origin of the cusped behavior in Re$C$ may be traced to the fact that cusps are also present in the absorptive part of $C$, Im$C$, as illustrated in Fig. 10. These cusps may be understood as Van Hove singularities, appearing because of the behavior of the available phase space for creating pair-breaking excitations of a given $k_{\parallel}$ and $\omega$. This behavior enters through the factor $\delta(\omega-E_{q+}-E_{q-})$ appearing in the integrands for Re$G$ and Re$F_{\pm}$ (cf. Appendix B), where $\mathbf{q}_{\pm}\equiv\mathbf{q}\pm\frac{1}{2}\mathbf{k}_{\parallel}$, and $\mathbf{q}$ is a two-dimensional momentum that must be integrated over. The values of $\mathbf{q}$ satisfying the $\delta$ function may be illustrated by the following geometric construction: on a $q_x$-$q_y$ plane, we draw two circles, one centered at $\mathbf{q}=\frac{1}{2}\mathbf{k}_{\parallel}$ (which for concreteness we take to lie on the $q_y$ axis), and the other centered at $-\frac{1}{2}\mathbf{k}_{\parallel}$. This is illustrated in Fig. 11. The radii of the circles, $q_1$ and $q_2$, are chosen such that $E_{q_1}=\varepsilon$ and $E_{q_2}=\omega-\varepsilon$, where $\varepsilon$ is a parameter that we al-

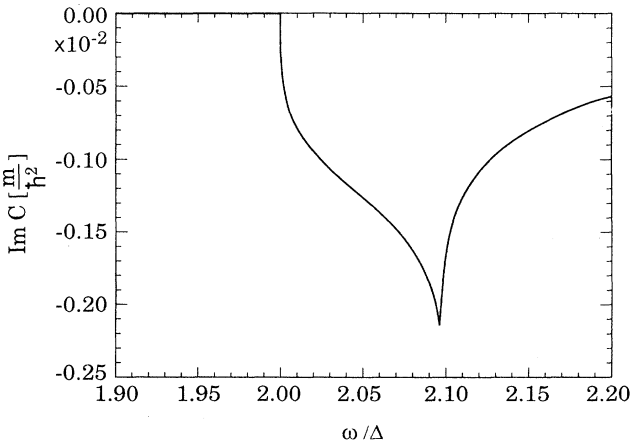


FIG. 10. Behavior of Im$C$ near $\omega=2\Delta$; parameters as in Fig. 9.

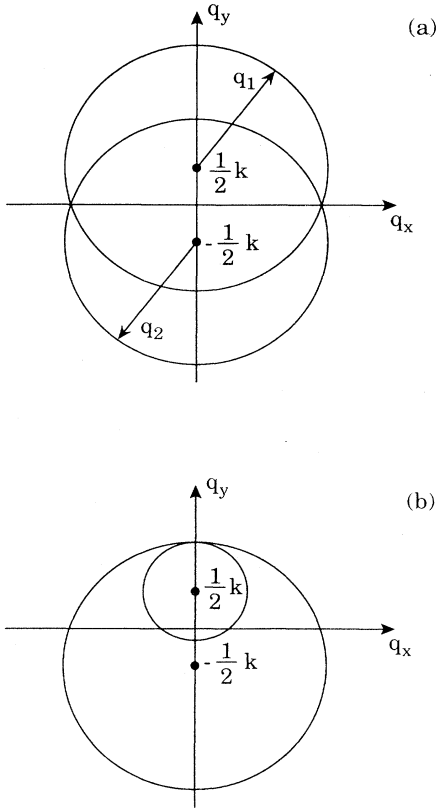


FIG. 11. Geometric construction that shows the allowed **q** vectors for a pair-breaking excitation with a given **k** and $\omega$. (a) Dotted lines show values of **q** that are allowed. (b) Situation in which the circles touch tangentially creates a Van Hove singularity.

low to vary over the range $\Delta \leq \varepsilon \leq \omega - \Delta$. It is clear that the locus of points $\mathbf{q}(\varepsilon)$ for which the two circles intersect represent values of **q** that satisfy the $\delta$ function. We see now that the slope discontinuity in Im$C$ arises because there is no allowed interval for $\varepsilon$ when $\omega < 2\Delta$. As $\varepsilon$ is increased above $2\Delta$, the allowed **q** values form a pair of arcs traced out across the $q_x$ axis [Fig. 11(a)]. The arcs get larger as $\omega$ is increased, until they meet at the $q_y$ axis when $\omega = \omega_c \equiv (4\Delta^2 + v_F^2 k_\parallel^2)^{1/2}$. If we increase $\omega$ above this, then for values of $\varepsilon > \omega_c - \Delta$, and also for values $\varepsilon < \Delta + (\omega - \omega_c)$, there are no points at which the two circles intersect. The critical point at which $\varepsilon = \omega_c - \Delta$ is illustrated in Fig. 11(b), where one can see that the two circles touch tangentially on the $q_y$ axis. It is this behavior that is characteristic of a Van Hove singularity, and it leads directly to the second cusp in Im$C(k_\parallel, \omega)$.

We see, finally, that the line splitting in Im$\chi$ is a result of Van Hove type singularities in the available density of state for pair-breaking excitations, amplified tremendously when the collective mode crosses the gap at $2\Delta$. The physical origin of this line splitting implies that it would be suppressed by disorder and finite temperatures, the former smoothing out the Van Hove singularities, and the latter effectively replacing the $\delta$ functions appearing in Re$G$ and Re$F_\pm$ with peaks with widths of order $k_B T$. Interplane tunneling, by contrast, does not smooth out the singularities, so that as long as the tunneling rate is small enough to allow modes to remain in the gap, one still expects to see the line splitting. The effect of tunneling on the plasmon dispersion—in particular, the extent to which one might still expect to have modes in the gap—is the subject of the next section.

## V. EFFECT OF INTERPLANE TUNNELING

In this section, we will derive the plasmon dispersions $\omega(\mathbf{k})$ when there is some degree of interplane tunneling. Our method of introducing tunneling is to put it directly in the single-particle spectrum:

$$\varepsilon(\mathbf{k}) = k_\parallel^2/2m - W\cos(k_z d) \ . \tag{18}$$

The formal development parallels that of Sec. II, and we will not run through the steps again. The results are given by Eqs. (2), (11), and (12), with the following modifications: (1) The integrals in Eqs. (2) are now three dimensional, rather than two dimensional, with $q_z$ integration running from $-\pi/d$ to $\pi/d$; (2) the quasiparticle energies $E_q \equiv \{\Delta^2 + [\varepsilon(\mathbf{k}) - \mu]^2\}^{1/2}$ must use the miniband approximation for $\varepsilon(\mathbf{k})$ in Eq. (18); and (3) the effective interaction is taken as

$$\tilde{v}(\mathbf{k}) = \frac{2\pi e^2 d}{\kappa k_\parallel} \frac{\sinh(k_\parallel d)}{\cosh(k_\parallel d) - \cos(k_z d)} - V_0 \ . \tag{19}$$

The extra factor of $d$ in the Coulomb interaction arises because, in this situation, we must use a three-dimensional rather than a two-dimensional Fourier transform. This form is appropriate when the width of the wells in which the electrons are confined is much smaller than the layer separation.

Since we are interested only in the plasmon dispersions in the gap, we will use the small-$k$ expansions, as in Sec. III, to find them. We note from the outset that, so long as a mode may be found in the gap, then as one increases $k$ such that the mode exits the gap, one will get strong mode-coupling effects when $\omega(\mathbf{k}) \simeq 2\Delta$, along with the line splitting in Im$\chi$ explained in detail in Sec. IV. Although there will be some changes in the details of the line shape, we expect its basic structure will be the same as in Sec. IV. The large amount of effort required to numerically generate $F_\pm$ and $G$ with the single-particle energies in Eq. (18) would only yield some detailed changes, and we believe no new physical insight would accompany it.

In the small-$k$ expansions, Eqs. (11) may be written as

$$\begin{aligned} G(\mathbf{k},\omega) &\cong -i[\Delta I_1(\omega) + K_1(\mathbf{k},\omega) \\ &\quad + (1/2\Delta) J_2(\mathbf{k},\omega)] + \mathcal{O}(k^2) \ , \\ F_+(\mathbf{k},\omega) &\cong i[2\Delta^2 I_1(\omega) + J_1(\mathbf{k},\omega) + J_2(\mathbf{k},\omega)] + \mathcal{O}(k^4) \ , \\ F_-(\mathbf{k},\omega) &\cong \frac{-i}{V_0} + \tfrac{1}{2} i\omega^2 I_1(\omega) \\ &\quad + i[I_2(\mathbf{k},\omega) + I_3(\mathbf{k},\omega)] + \mathcal{O}(k^4) \ . \end{aligned} \tag{20}$$

The exact forms of the functions $I_1$, $I_2$, $I_3$, $J_1$, and $K_1$ are detailed in Appendix C. To find the plasmon modes, we need to set the denominator of Eq. (2) to zero. Using Eqs. (11) and (20), this yields

$$\tfrac{1}{4}\omega^2+\frac{I_2+I_3}{2I_1} =\bar{v}(\mathbf{k})[2\Delta^2(I_2+I_3)+\tfrac{1}{2}\omega^2(J_1-J_2)-2\omega^2\Delta J_1]\ , \quad (21)$$

where $\bar{v}(\mathbf{k})$ appears in Eq. (19). For a fixed value of $\mathbf{k}$, the value of $\omega$ satisfying Eq. (21) is the plasmon frequency $\omega(\mathbf{k})$. We note that, as in Sec. III, our expansions become invalid when $\omega \geq 2\Delta - v_F k_\parallel/2$; in the long-wavelength limit, this only limits us in a small interval below the gap edge.

In Fig. 4, we plot $\omega(\mathbf{k})$ for fixed $k_z d=\pi/100$ as a function of $k_\parallel d$. One can see that, at smaller values of $W$, the major effect of tunneling is to open a small gap near $k_\parallel d=0$. For larger values of $W$ (e.g., $W=0.1\Delta$ in Fig. 4), we see that entire dispersion $\omega(\mathbf{k})$ is pushed up to slightly higher energies. It is easy to see that, for large enough $W$, the entire plasmon mode may be pushed out of the gap. It is also interesting to consider how the phase diagram illustrated in Fig. 2 is modified by the presence of tunneling. Unfortunately, for $W\neq 0$, it becomes difficult to meaningfully extrapolate the dispersions to $\omega=2\Delta$, especially when $k_z d$ is large, which is actually the region most affected by interplane tunneling. However, we can get an idea of what happens by plotting the locus of points at which $\omega(\mathbf{k})=1.6\Delta$, for which our expansions are perfectly valid, for different values of $W$. Clearly, these curves will be very similar to the "phase boundaries" given by $\omega(\mathbf{k})=2D$. This is illustrated in Fig. 12. One can see that the curves move inward towards $\mathbf{k}=0$ as $W$ is increased; the initial slope of the curve also decreases with increasing $W$. This latter behavior indicates that the critical angle $\theta_c$ is a decreasing function of $W$, as expected. (Recall that modes propagating in a direction $\theta<\theta_c$ with respect to the superlattice axis will always lie in the gap at small enough $|\mathbf{k}|$; this is the definition of $\theta_c$.) In Fig. 13, we plot $\theta_c$ as a function of $W$; note that here we have been able to extrapolate essentially all the way to $2\Delta$, because the range over which our expansions begin to fail ($v_F k_\parallel/2$) is vanishingly small. As stated in the Introduction, we find that $\theta_c \approx 8°$ for $W=0$, and $\theta_c$ vanishes at $W\simeq 0.23\Delta$. Note that the vanishing of $\theta_c$ indicates that all modes have exited the gap; within our approximations, for the sample parameters indicated in Fig. 1, there are no modes in the gap when $W>0.23\Delta$. If we estimate $W$ from the effective mass approximation, we find $W\simeq 1/m_z d^2$, and using a mass anisotropy of $r\equiv m_z/m_\parallel=100$, and $M_\parallel \simeq 5m_0$ (as would be appropriate for Y-Ba-Cu-O), with $m_0$ the bare electron mass, we find $W\simeq 0.0075\Delta$, for $d\simeq 10$ Å and $\Delta$ given by the BCS formula with $T_c\simeq 125$ K. Thus, we find that, in this estimate, our hypothetical superconductor (roughly modeling Y-Ba-Cu-O) should be well inside a region where modes can propagate inside the gap. We note, however, that the effective mass approximation is not actually valid at the densities we consider, so that the value of $W$ obtained this way is somewhat suspect; however, so long as this estimate is within a factor of 30 of the actual value of $W$, we still expect there to be collective modes in the gap. It is important to notice that the case for having modes in the gap for Bi-based and Tl-based compounds is even stronger, where the measured mass anisotropies have reached $r=3\times 10^3$ in the former case[2], and $r>10^5$ in the latter.[3]

Finally, it is important to note that estimates based directly on the effective-mass approximation[14] for modes propagating along the $\hat{\mathbf{z}}$ direction—i.e., $\omega_p^2=4\pi e^2\rho/m_z$—may grossly overestimate the long-wavelength limit for the $\theta=0$ mode. For example, if we use this estimate with the parameters listed in Fig. 1, and $m_z=5rm_0$, with $r=100$, we find $\omega_p\simeq 1.4\Delta$, which is over an order of magnitude larger than our estimate based

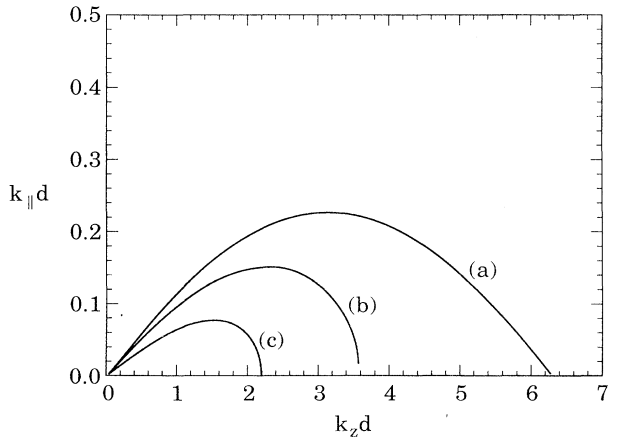


FIG. 12. Values of $\mathbf{k}$ for which $\omega(\mathbf{k})=1.6\Delta$, for different values of tunneling parameter $W$. Material parameters as in Fig. 1, with (a) $W=0$, (b) $W=0.1\Delta$, and (c) $W=0.15\Delta$. Curves are expected to be qualitatively the same as phase diagram separating modes below the gap edge at $2\Delta$ from those above it.

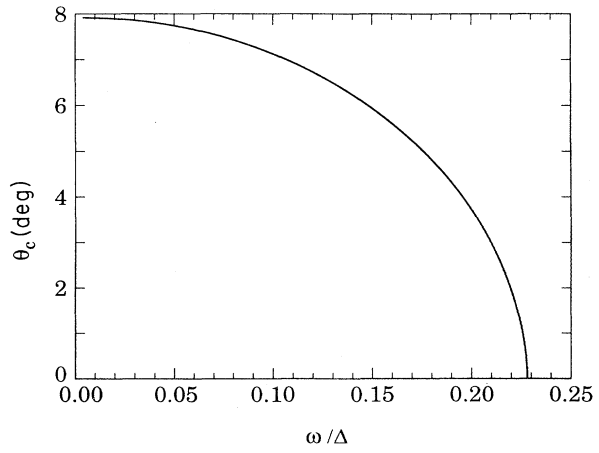


FIG. 13. Critical angle, in degrees, of long-wavelength modes as a function of tunneling rate, $W$.

directly on Eq. (21) (see Fig. 4). Thus, such rough estimates tend to be unreasonably pessimistic about whether one can find modes in the gap when the tunneling between planes is small.

## VI CONCLUSION

In this work, we have shown that layered superconductors can support low-energy collective excitations, such that, for wave vectors $\mathbf{k}$ directed close to the superlattice axis, the plasmon energy $\omega(\mathbf{k})$ may be *smaller* than the gap energy, $2\Delta$, in the long-wavelength limit. This is an unusual situation because, for isotropic superconductors, the collective-mode energies are well above the gap. We find that as the plasmon dispersion crosses the gap edge at $2\Delta$—either by increasing $\mathbf{k}$, or by tilting the angle of $\mathbf{k}$ with respect to the superlattice axis—an unusual mode coupling occurs between the collective excitations and the pair-breaking excitations. The mode coupling leads to a line splitting in the absorptive part of the dielectric response. We find that one of the peaks in the line shape is always maximum at $2\Delta$, suggesting that if one can detect the collective mode, then one can uniquely identify the gap as the mode passes through the gap edge at $2\Delta$. Finally, we have considered the effect of interplane tunneling on the collective-mode spectrum; we find that, as the tunneling between planes is increased, the plasmon modes are pushed up in energy. Our rough estimates for this tunneling rate suggest that, for most high-$T_c$ materials, the interplane tunneling is not strong enough to push the plasmon mode out of the gap. Finally, we note that estimates for the plasmon energy based on the effective-mass approximation can grossly overestimate this energy when the interplane tunneling is weak.

## ACKNOWLEDGMENTS

The authors would like to thank many colleagues for helpful discussions, including R. E. Prange, D. Belitz, S. K. Yip, H. D. Drew, and Thi Pham. This work was supported by the NSF, the U.S. ONR, and U.S. ARO. Computer time was provided by University of Maryland.

## APPENDIX A: SMALL-$k_\parallel$ EXPANSIONS OF $F_\pm$ AND $g$ IN THE ABSENCE OF TUNNELING

Equations (12) may be directly expanded in $k_\parallel^2$ when $\omega<2\Delta$, and the resulting integrals may be handled analytically. We find

$$G(k_\parallel,\omega)\cong\frac{im\Delta}{2\pi x\omega}\arctan u+\frac{im\Delta}{8\pi}\left\{\frac{1}{8x^2\Delta^2u}\left[\frac{5}{3}\frac{1}{u}+\frac{1}{u^3}-\left[1+\frac{1}{u^2}\right]^2\arctan u\right]\right.$$
$$+\frac{1}{4x^2\Delta^2u^3}\left[\frac{2}{3}u+\frac{1}{u}-\left[1+\frac{1}{u^2}\right]\arctan u\right]$$
$$\left.-\frac{1}{8x^4u^2}\left[\frac{3}{u^2}+1-\frac{1}{u}(1+u^2)\left[\frac{3}{u^2}-1\right]\arctan u\right]\right\}(v_Fk_\parallel)^2\,, \tag{A1}$$

$$F_+(k_\parallel,\omega)\cong\frac{-im\Delta^2}{\pi x\omega}\arctan u+\frac{2im\Delta^2}{\pi}\left[\frac{-1}{u\omega^2\Delta^2}\left[\frac{2}{3}u+\frac{1}{u}-\frac{\Delta^2}{x^2}\frac{1}{u^2}\arctan u\right]\right.$$
$$+\frac{u}{4\omega^2\Delta^2}\left[\frac{5}{3u}+\frac{1}{u^3}-\frac{\Delta^4}{x^4u^4}\arctan u\right]$$
$$\left.+\frac{1}{8x^4u^4}+\frac{\Delta^2}{16x^6u^4}-\frac{\Delta^2}{8x^6u^3}\left[\frac{3}{2u^2}-\frac{1}{2}\right]\arctan u\right](v_Fk_\parallel)^2\,, \tag{A2}$$

$$F_-(k_\parallel,\omega)\cong\frac{-i}{V_0}-\frac{im\omega}{4\pi x}\arctan u+\frac{im}{2\pi}\left\{\frac{1}{4x^2u}\left[\left[1+\frac{1}{u^2}\right]\arctan u-\frac{1}{u}\right]\right.$$
$$\left.+\frac{\Delta^2}{2ux^4}\left[\frac{1}{2u}+\frac{1}{2}\left[1-\frac{1}{u^2}\right]\arctan u\right]\right\}(v_Fk_\parallel)^2\,, \tag{A3}$$

where $x^2\equiv\Delta^2-\omega^2/4$ and $u\equiv\omega/2x$. These expressions are well behaved for $\omega<2\Delta-v_Fk_\parallel/2$. In the interval $2\Delta-v_Fk_\parallel/2\le\omega\le2\Delta$, they increase sharply and are divergent at $\omega=2\Delta$. For $\omega>2\Delta$, they are invalid. Because the wavelengths of interest to us are long, we have $v_Fk_\parallel/2\ll2\Delta$, so that the nonanalytic behavior near $2\Delta$ does not present a problem, so long as we apply these results only to the dielectric response for frequencies below the gap edge.

## APPENDIX B: Re$F_\pm$ AND Re$G$ IN TERMS OF ELLIPTIC INTEGRALS

The real parts of the quantities $F_\pm$ and $G$ may be expressed as one-dimensional integrals because we may write $\mathrm{Im}\{1/[\omega\pm(E_{q+}+E_{q-}-i\delta)]\}=\mp\pi\delta(\omega\pm(E_{q+}+E_{q-}))$ in Eqs. (12), allowing the angular integration to be performed

analytically. After a great deal of algebra, we find these integrals may be written most completely as

$$\begin{aligned}
\mathrm{Re}G(k_\parallel,\omega)&=\frac{-m\Delta}{4\pi}\int_a^1\frac{dx}{(1-x^2)^{1/2}(\alpha-\beta x^2)^{1/2}}\ ,\\
\mathrm{Re}F_+(k_\parallel,\omega)&=-\frac{m}{2\pi}\int_a^1 dx\frac{2x^2y_0^2-\frac{1}{2}\omega^2}{(1-x^2)^{1/2}(\alpha-\beta x^2)^{1/2}}\ ,\\
\mathrm{Re}F_-(k_\parallel,\omega)&=-\frac{m\omega^2\Delta^2}{4\pi y_0^2}\int_a^1 dx\frac{1}{(\omega^2/4y_0^2-x^2)(1-x^2)^{1/2}(\alpha-\beta x^2)^{1/2}}\ ,
\end{aligned}\tag{B1}$$

for $\omega>2\Delta$, where $\alpha\equiv\omega^2(E_Fk_\parallel^2/2m-y_0^2)$, $\beta=y_0^2(2E_Fk_\parallel^2/m-\omega^2)$, $y_0^2\equiv\omega^2/4-\Delta^2$, and $a=0$ for $\omega^2\le4(E_Fk_\parallel^2/2m+\Delta^2)$, $a=|\alpha/\beta|^{1/2}$ for $\omega^2>4(E_Fk_\parallel^2/2m+\Delta^2)$.

For $\alpha,\beta>0$, these take the form

$$\begin{aligned}
\mathrm{Re}G=\frac{m\Delta}{4\pi\omega^2}&\left[\left(\frac{\omega^2}{\alpha^{1/2}}-\frac{4y_0^2\alpha^{1/2}}{\beta}\right)F(\zeta,t)\right.\\
&+\frac{4y_0^2\alpha^{1/2}}{\beta}E(\zeta,t)\\
&\left.-4ay_0^2\left(\frac{1-a^2}{\alpha-\beta a^2}\right)^{1/2}\right]\ ,\\
\mathrm{Re}F_+=-\frac{m}{2\pi}&\left[\frac{2y_0^2}{\beta^{1/2}}\left(\frac{\alpha}{\beta}\right)^{1/2}[F(\zeta,t)-E(\zeta,t)]\right.\\
&-\frac{1}{2}\frac{\omega^2}{\alpha^{1/2}}F(\zeta,t)\\
&\left.+2ay_0^2\left(\frac{1-a^2}{\alpha-\beta a^2}\right)^{1/2}\right]\ ,\\
\mathrm{Re}F_-=\frac{m\omega^2\Delta^2}{4\pi|\alpha|^{1/2}}&\frac{16y_0^2}{[\omega^2-4(\alpha/\beta)y_0^2](\omega^2-4y_0^2)}\\
\times&\left[\left(1-\frac{\alpha}{\beta}\right)\Pi\left(\zeta,\frac{\omega^2\beta-4\alpha y_0^2}{\omega^2\alpha-4y_0^2},t\right)\right.\\
&\left.+\left(\frac{\omega}{4y_0^2}-1\right)F(\zeta,t)\right]\ ,
\end{aligned}\tag{B2}$$

where $F$, $E$, and $\Pi$ are elliptic integrals of the first, second, and third kinds, respectively, $t=(\beta/\alpha)^{1/2}$, and $\sin\zeta=[\alpha(1-a^2)/(\alpha-\beta a^2)]^{1/2}$. For $\alpha>0$, $\beta<0$, we find

$$\begin{aligned}
\mathrm{Re}G=\frac{m\Delta}{4\pi\omega^2|\beta|^{1/2}}&\left[\frac{\omega^2+4y_0^2|\alpha/\beta|}{(|\alpha/\beta|+1)^{1/2}}F(\delta,r)\right.\\
&\left.-4y_0^2(1+|\alpha/\beta|)^{1/2}E(\delta,r)\right]\ ,\\
\mathrm{Re}F_+=-\frac{m}{2\pi}&\left\{\frac{2y_0^2}{|\beta|^{1/2}}\left[\left(\frac{\alpha+|\beta|}{|\beta|}\right)^{1/2}E(\delta,r)\right.\right.\\
&\left.-\frac{\alpha/|\beta|^{1/2}}{(\alpha+|\beta|)^{1/2}}F(\delta,r)\right]\\
&\left.-\frac{1}{2}\omega^2\frac{1}{(\alpha+|\beta|)^{1/2}}F(\delta,r)\right\}\ ,\\
\mathrm{Re}F_-=\frac{m\omega^2}{4\pi}&\frac{1}{(\alpha+|\beta|)^{1/2}}\Pi\left(\delta,-\frac{y_0^2}{\Delta^2}r\right)\ ,
\end{aligned}\tag{B3}$$

where $\cos\delta=a$, $r=1/(|\alpha/\beta|+1)^{1/2}$. Finally, for $\alpha<0$, $\beta<0$, we find

$$\begin{aligned}
\mathrm{Re}G&=\frac{\Delta m}{4\pi|\beta|^{1/2}}\left[F(\lambda,s)-4\frac{y_0^2}{\omega^2}E(\lambda,s)\right]\cdot,\\
\mathrm{Re}F_+&=-\frac{m}{2\pi|\beta|^{1/2}}[2y_0^2E(\lambda,s)-\tfrac{1}{2}\omega^2F(\lambda,s)]\ ,\\
\mathrm{Re}F_-&=\frac{m\omega^2}{4\pi|\beta|^{1/2}}\Pi\left(\lambda,\frac{1-|\alpha/\beta|}{1-\omega^2/4y_0^2},s\right)\ ,
\end{aligned}\tag{B4}$$

where $\sin\lambda=[(1-a^2)/(1-|\alpha/\beta|)]^{1/2}$ and $s=(1-|\alpha/\beta|)^{1/2}$. Note that, in all three cases, $\mathrm{Re}G=(4\Delta/\omega^2)\mathrm{Re}F_+$; however, because the Kramers-Kroenig transform is a frequency integral, the imaginary parts of these will not, in general, obey a simple relationship.

## APPENDIX C: FORMS FOR $I_1, I_2, I_3, J_1, J_2$, AND $K_1$

Integrals involved in computing $\mathrm{Im}F_\pm$ and $\mathrm{Re}G$ when tunneling between planes is allowed may be evaluated in a fashion similar to that described in Appendix A. We find that the integrations with respect to $q_x$ and $q_y$ may be handled analytically; the integrations over $q_z$ must be performed numerically. The latter is not difficult, however, because the integrands are very well behaved, and hence may be handled with standard integration packages. We find that the functions are conveniently parametrized as shown in Eq. (20), with

$$I_1(\omega)=-\frac{m}{8\pi^2}\frac{1}{\omega x}\left[2\pi\arctan u+\int_{-\pi}^{\pi}dz\arctan v_0(z)\right]\ ,\tag{C1}$$

$$I_2(\mathbf{k},\omega)=\frac{m}{(2\pi)^2 d}\int_{-\pi}^{\pi} dz\,\beta(z)\left\{\frac{1}{4\omega x}\left[\arctan u+\arctan v_0(z)-\frac{1}{u^2}(u+v_0-\arctan u-\arctan v_0)\right]\right.$$
$$+\frac{\Delta^2}{16\omega x^3}\left[\left[1-\frac{1}{u^2}\right](\arctan u+\arctan v_0)+\left[1+\frac{1}{u^2}\right]\left[\frac{v_0}{1+v_0^2}+\frac{\omega x}{2\Delta^2}\right]\right]$$
$$+\frac{\omega}{32x^3}\left[\frac{1}{2}\left[1\frac{2}{u^2}-\frac{3}{u^4}\right](\arctan u+\arctan v_0)\right.$$
$$\left.\left.+\frac{1}{2}\left[1+\frac{1}{u^2}\right]^2\left[\frac{\omega x}{2\Delta^2}+\frac{v_0}{1+v_0^2}\right]+\frac{1}{u^4}(v_0+u)\right]\right\}, \tag{C2}$$

$$I_3(\mathbf{k},\omega)=\frac{m}{(2\pi)^2 d}\int_{-\pi}^{\pi} dz\,b(z)\left[-\frac{1}{2\omega}\ln\frac{1+v_1(z)}{1-v_1(z)}-\frac{W\cos z}{x\omega}[\arctan u+\arctan v_0(z)]\right.$$
$$\left.+\frac{1}{\omega}\left[\tfrac{1}{2}\ln\frac{1+v_1}{1-v_1}+\frac{v_1}{1-v_1^2}\right]+\frac{\Delta^2 W\cos z}{\omega x^3}\left[\arctan u+\arctan v_0+\frac{u}{1+u^2}+\frac{v_0}{1+v_0^2}\right]\right], \tag{C3}$$

$$J_1(\mathbf{k},\omega)=\frac{m}{(2\pi)^2 d}\int_{-\pi}^{\pi} dz\,\beta(z)\left\{\frac{3}{8\omega x}\left[\left[1+\frac{1}{u^2}\right]^2[\arctan u+\arctan v_0(z)]\right.\right.$$
$$\left.+\frac{1}{u^4}\left[\frac{u^3}{3}+\frac{v_0^3}{3}\right]-\left[\frac{2}{u^2}+\frac{1}{u^4}\right](u+v_0)\right]$$
$$-\frac{1}{2\omega x}\left[\left[1+\frac{1}{u^2}\right](\arctan u+\arctan v_0)-\frac{1}{u^2}(u+v_0)\right]$$
$$+\frac{\Delta^2}{4\omega x^3}\left[\tfrac{1}{2}\left[1+\frac{1}{u^2}\right]\left[1-\frac{3}{u^2}\right]\arctan u+\arctan v_0)\right.$$
$$\left.\left.+\tfrac{1}{2}\left[1+\frac{1}{u^2}\right]^2\left[\frac{u}{1+u^2}+\frac{v_0}{1+v_0^2}\right]+\frac{1}{u^4}(v_0+u)\right]\right\}, \tag{C4}$$

$$J_2(\mathbf{k},\omega)=\frac{m\Delta^2}{(2\pi)^2 d}\int_{-\pi}^{\pi} dz\,b(z)\left[\frac{4}{\omega^3}\left[\frac{v_1(z)}{1-v_1^2(z)}-v_1(z)\right]\right.$$
$$\left.+\frac{W\cos z}{\omega x}\left\{\left[\left[1-\frac{1}{u^2}\right]\frac{1}{x^2}+\left[1+\frac{1}{u^2}\right]\frac{1}{\Delta^2}\right][\arctan u+\arctan v_0(z)]\right.\right.$$
$$\left.\left.+\frac{1}{x^2}\left[1+\frac{1}{u^2}\right]\left[\frac{u}{1+u^2}+\frac{v_0}{1+v_0^2}\right]-\frac{1}{\Delta^2 u^2}(u+v_0)\right\}\right], \tag{C5}$$

$$K_1(\mathbf{k},\omega)=\frac{1}{2\Delta}\left[J_1(\mathbf{k},\omega)+\frac{m}{(2\pi)^2 d}\frac{1}{4\omega x}\int_{-\pi}^{\pi} dz\,\beta(z)\left[\arctan u+\arctan v_0(z)-\frac{1}{u^2}(u+v_0-\arctan u-\arctan v_0\right]\right], \tag{C6}$$

where $x\equiv(\Delta^2-\omega^2/4)^{1/2}$, $u\equiv\omega/2x$, $v_0(z)\equiv y_0 u/(y_0^2+\Delta^2)^{1/2}$, $v_1(z)\equiv\omega/2(\Delta^2+y_0^2)^{1/2}$, $y_0(z)\equiv E_F+W\cos z$, $\beta(z)\equiv y_0(z)k_\parallel^2/m+(Wk_z d\sin z)^2$, and $b(z)=\frac{1}{8}[k_\parallel^2/m+(W\cos z)(k_z d)^2]$. One may check that, with these expressions, Eqs. (20) reduce to the forms shown in Appendix A for $F_\pm$ and $G$ when $W\to 0$, as we expect. Note that $I_2$, $I_3$, $J_1$, $J_2$, and $K_1$ all vanish when $k_\parallel, k_z\to 0$.


[1]For a review, see W. E. Pickett, Rev. Mod. Phys. **61**, 433 (1989), and references therein.
[2]D. E. Farrell *et al.*, Phys. Rev. Lett. **63**, 782 (1989).
[3]D. E. Farrell *et al.* (unpublished).
[4]N. Missert and M. R. Beasley, Phys. Rev. Lett. **63**, 672 (1989).
[5]S. Das Sarma and J. J. Quinn, Phys. Rev. B **25**, 7603 (1982).
[6]P. Olego, A. Pinczuk, A. C. Gossard, and W. Wiegmann, Phys. Rev. B **31**, 2578 (1985)
[7]H. A. Fertig and S. Das Sarma, Phys. Rev. Lett. **65**, 1482 (1990).

[8]P. W. Anderson, Phys. Rev. **122**, 1900 (1958); G. Rickayzen, *ibid.* **115**, 729 (1959).

[9]S. Doniach and M. Invi, Phys. Rev. B **41**, 6668 (1990) obtained a similar result in the context of a phenomenological Ginzburg-Landau theory. Our work, by contrast, starts with a microscopic Hamiltonian, and is more appropriate near $T=0$.

[10]R. E. Prange, Phys. Rev. **129**, 2495 (1963).

[11]D. Belitz, S. De Souza-Machado, T. P. Devereaux, and D. W. Hoard, Phys. Rev. B **39**, 2072 (1989).

[12]R. Zeyher and G. Zwicknagl, Z. Phys. B **78**, 175 (1990) predict a similar phenomenon when there is an accidental crossing between optical phonon modes and the energy gap, $2\Delta$.

[13]T. M. Mishonov (unpublished).

[14]G. L. Doll *et al.*, Phys. Rev. B **38**, 8850 (1988).

[15]Z. Schlesinger *et al.*, Phys. Rev. Lett. **65**, 801 (1990).

[16]Y. Nambu, Phys. Rev. **117**, 648 (1960).

[17]J. R. Schrieffer, *Theory of Superconductivity* (Benjamin, Reading, 1964).

[18]We thank S. K. Yip for a discussion on this point.

[19]D. Belitz (private communication).

[20]The dielectric response of layered superconductors has been discussed recently by J. J. Chang and D. Scalapino, Phys. Rev. B **40**, 4299 (1989); H. Chen *et al.*, *ibid.* **43**, 383 (1991); however, neither of these approaches includes vertex corrections, and hence would be unable to get the correct collective-mode spectrum.